Ultrahigh-Performance of Li/Na Ion Batteries Using N/O Dual Dopants Porous Hollow Carbon Nanocapsules as Anode

Linlin Wang,*[#a] Bo Lu,[#b] Saisai Wang,[a,c] Wei Cheng,[d] Yufeng Zhao[a] Jiujun Zhang*[a] and Xueliang Sun*[e]

[a]*Institute for Sustainable Energy/College of Science, Shanghai University, 99 Shangda Road, Shanghai 200444, P.R. China. *E-mail:wlinlin@mail.ustc.edu.cn; jiujun.zhang@i.shu.edu.cn; xsun9@uwo.ca..*

[b]*Shanghai Institute of Applied Mathematics and Mechanics, Shanghai University, 149 Yanchang Road, Shanghai 200072, China..*

[c]*College of Chemistry and Chemical Engineering, Shanghai University of Engineering Science,333 Longteng Road, Shanghai, 201620, P.R. China.*

[d]*Department of Chemistry, The University of British Columbia, 2036 Main Mall, Vancouver, British Columbia V6H1Z1, Canada.*

[e]*Department of Mechanical and Materials Engineering, University of Western Ontario, 1151 Richmond St, London, Ontario, N6A 3K7, Canada.*

Theoretical calculations

Considering the diffusion driven by concentration gradient, transportation of Li in the active material is governed by Fick's law

$$\frac{\partial c}{\partial t} = D\nabla^2 c \qquad (1)$$

where c is the molar concentration of Li, and D is the diffusivity. The initial condition is assumed to be uniform, i.e.,

$$c = c_0 \quad \text{for} \quad t = 0. \qquad (2)$$

It is assumed that the electrical current density over the inner and outer surfaces is uniform. Therefore, the boundary conditions for galvanostatic operation could be given by

$$\mathbf{n} \cdot D\nabla c = \frac{i_n}{F} \quad \text{for all surfaces} \qquad (3)$$

where $\mathbf{n}$ stands for the direction vector of the surface, and i_n stands for the surface current density and F = 96485.3 *C/mol* is Faraday constant.

The equilibrium equation in terms of mechanical stress without body force is given by

$$\sigma_{ij,j} = 0 \quad . \tag{4}$$

And the kinematic relation between strain ε and displacement u is given by

$$\varepsilon_{ij} = \frac{1}{2}\left(u_{i,j} + u_{j,i}\right) \tag{5}$$

We assume that the active material undergoes elastic deformation during cell charging and discharging. The isotropic elastic constitutive equation for the active material reads as

$$\sigma_{ij} = \frac{E}{1+\upsilon}\varepsilon_{ij} + \frac{E\upsilon}{(1+\upsilon)(1-2\upsilon)}\varepsilon_{kk}\delta_{ij} - \frac{E}{1-2\upsilon}\frac{\Omega c}{3}\delta_{ij} \tag{6}$$

where σ_{ij} and ε_{ij} are stress and strain tensor, υ, E and Ω are Poisson's ratio, Young's modulus and the partial molar volume of the active material, respectively, δ_{ij} is the Kronecker delta. Moreover, the surfaces of the active material are assumed to be free, i.e.

$$\sigma_{ij} n_j = 0 \quad \text{for all surfaces.} \tag{7}$$

It is very difficult to obtain analytical solutions of diffusion-induced stresses due to the complex geometry. To obtain the numerical solutions, we carried out finite element calculations using the commercial package COMSOL-Multiphysics basing on above model. The diffusion-induced volumetric expansion is simulated as if it were thermal expansion. The transient (time dependent) solver was selected to compute the intercalation/extraction process.

The value of Young's modulus E is 30 Gpa,[S1] diffusivity D is 1×10^{-15} m^2/s,[S2] the partial molar volume Ω is 3.56×10^{-6} m^3/mol,[S1] and Poisson's ratio υ is chosen as 0.3.[S1-S3] The surface current density i_n is chosen as 60 A/m^2 for intercalation, while it is -60 $/m^2$ for extraction. The outer radius is 50 nm. The constant initial concentration c_0 has no contribution to the diffusion-induced stress and therefore can be assumed to be zero. Due to the significant small thickness (15 nm) as well as the length (700 nm), the hoop stress is the most important stress component in the specified tubular structure.

Fig.6 (a, b) (main text) demonstrates the distribution of hoop stress in the sealed hollow capsule, while Figure 6 c, d demonstrates that in the open-end one. Figs. 6a and 6c are axisymmetric cross-section figures, while Figs. 6b and 6d are 3D rotation figures. The figures only show the region with z < 350 nm, since the structure is symmetric. Due to the concentration gradient in intercalation, the hoop stress is compressive in the region near the surfaces, while it is tensile in the inner region, which is consistent with the results presented in references.[S4-S6] Since the current has an opposite sign in extraction, the stress is simply of opposite sign. The difference in the structure surely leads to the different maximum stress which takes responsibility for the mechanical damage.

Fig. 6e (main text) plots the maximum hoop stress against the intercalation/extraction time. It is found that the stress increases to its peak value then decreases to a steady-state value for both structures and both operations. However, the peak stress for the sealed hollow capsule is much lower than that for open-end one. Since higher

stress commonly leads to higher risk of mechanical degradation, it can be concluded that the sealed hollow capsule has better mechanical stability.

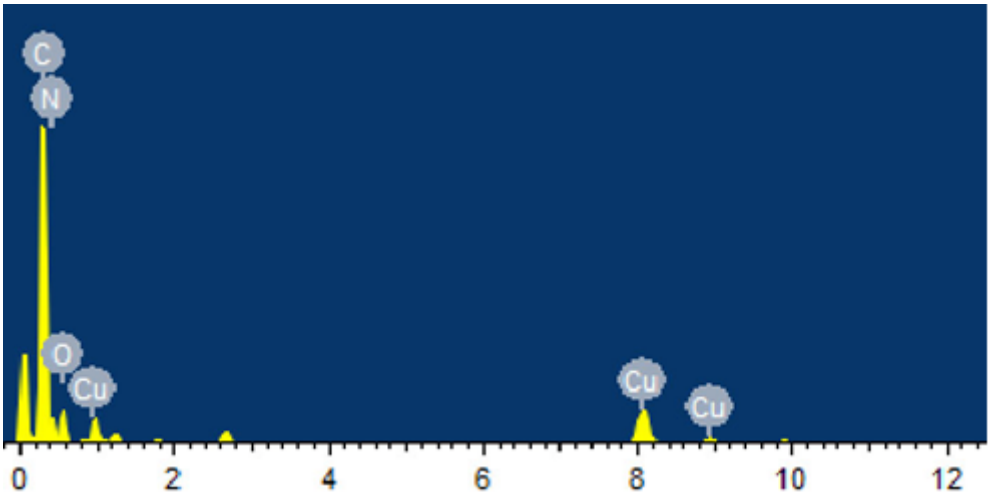

Fig. S1 EDS spectrum of the N/O-CNCs-600

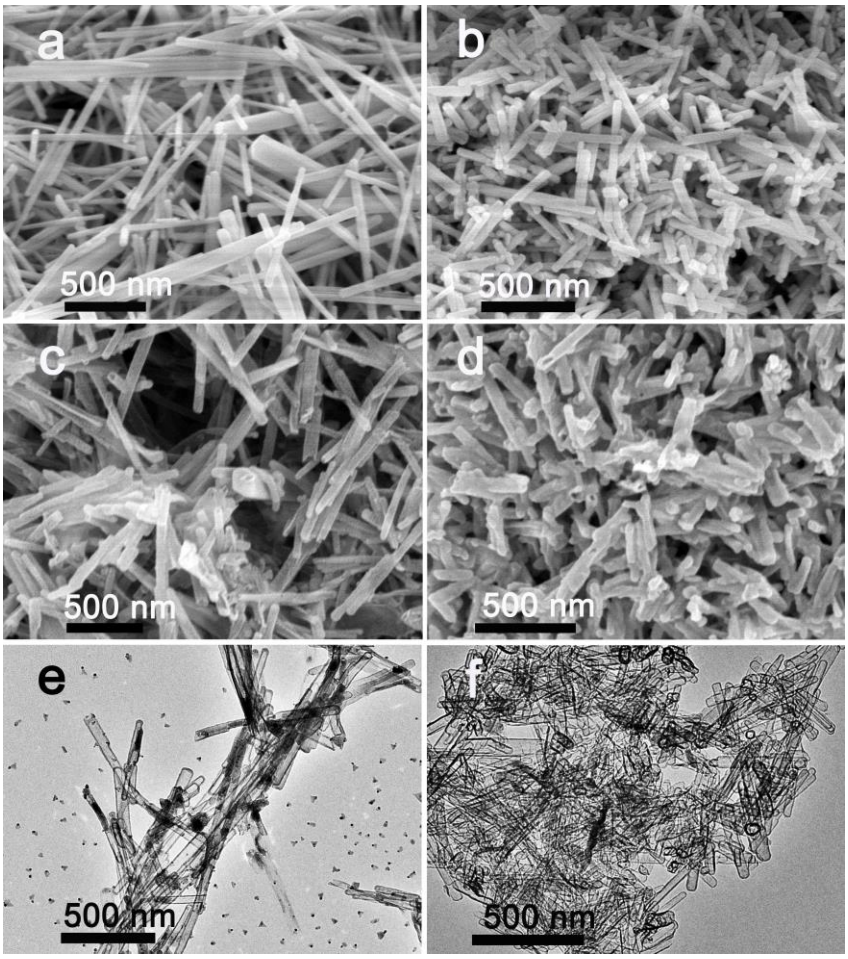

Fig. S2 SEM images of the Zn_2GeO_4 nanorodes (template) obtained with different pH

of: (a) 7.5, (b) 8.5~9. The corresponding SEM and TEM images of the N/O-CNCs obtained by the above templates: (c, e) and (d, f), respectively.

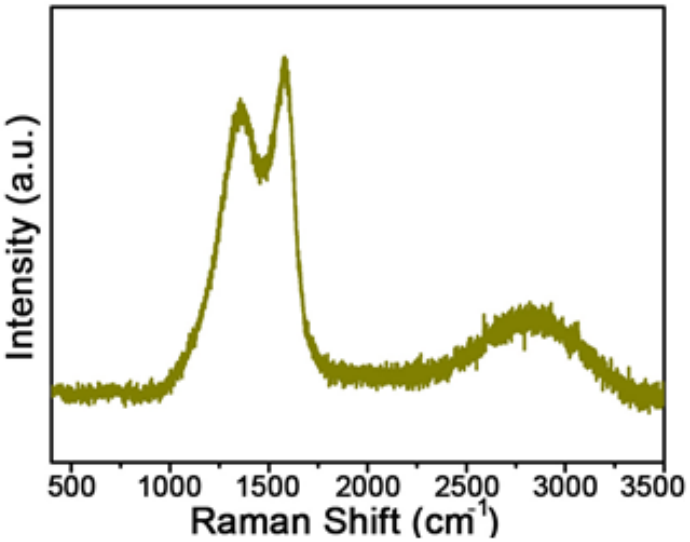

Fig. S3 Raman spectrum of the N/O-CNCs-600.

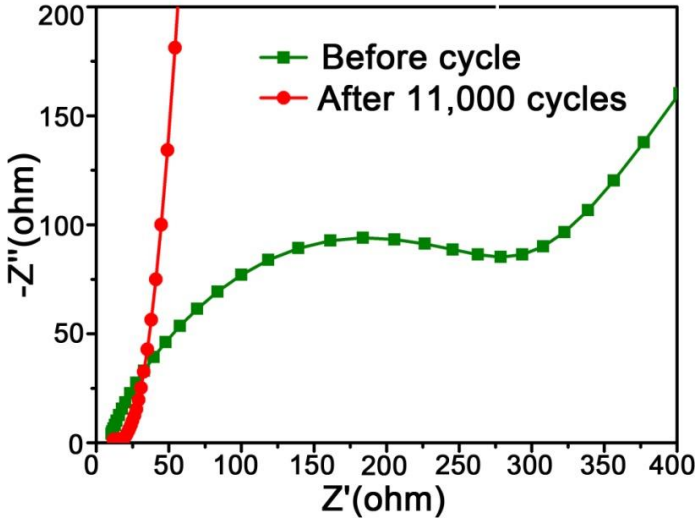

Fig.S4 Nyquist plots of the N/O-CNCs-600 electrodes before and after 11, 000 cycles.

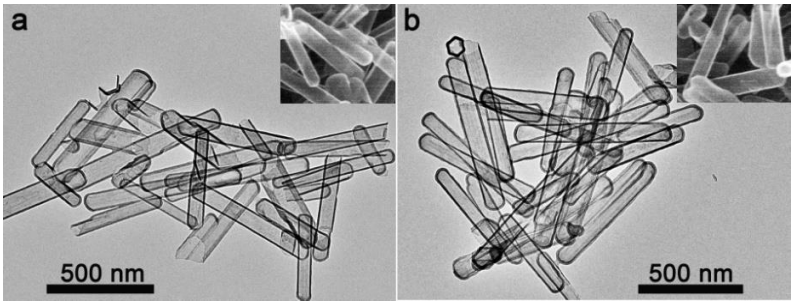

Fig. S5 TEM and SEM (inset) images of the carbonized samples(N/O-CNCs-500,

N/O-CNCs-700) obtained at different calcination temperatures: (a) 500 °C and (b) 700 °C, respectively.

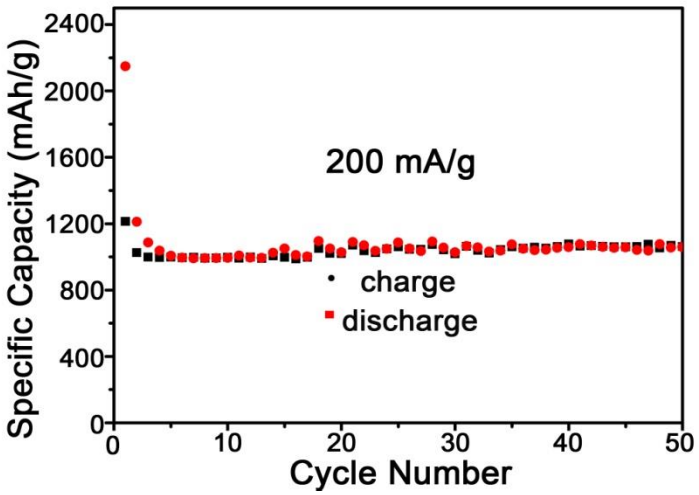

Fig.S6 Cycling performance of the N/O-CNCs-500 electrode at 200 mA/g.

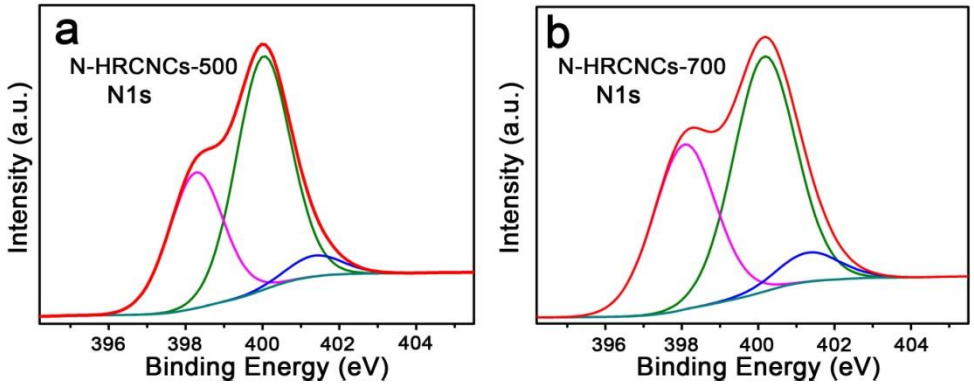

Fig. S7 N1s spectra of the N/O-CNCs (N/O-CNCs-500, N/O-CNCs-700) obtained at different carbonization temperatures: (a) 500 °C and (b) 700 °C, respectively.

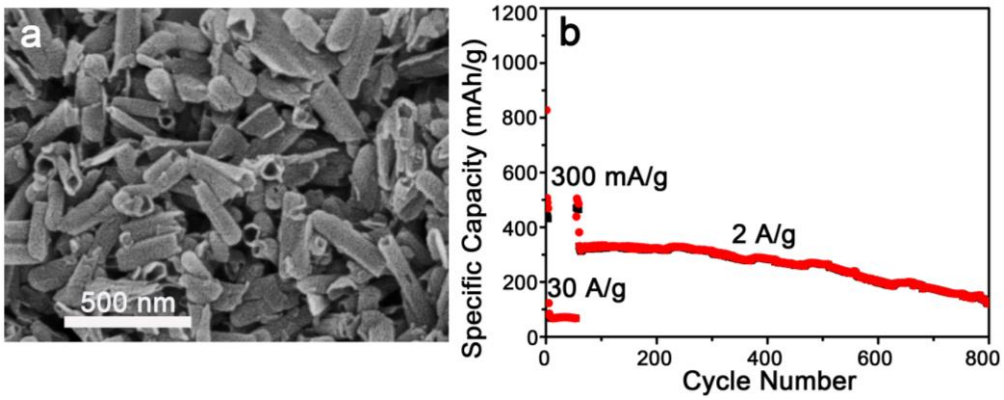

Fig. S8 (a) SEM image of the sample obtained by grinding. (b) Electrochemical

performances of the comparison electrode. (The density was set at 0.3 A/g for the fourth cycle).

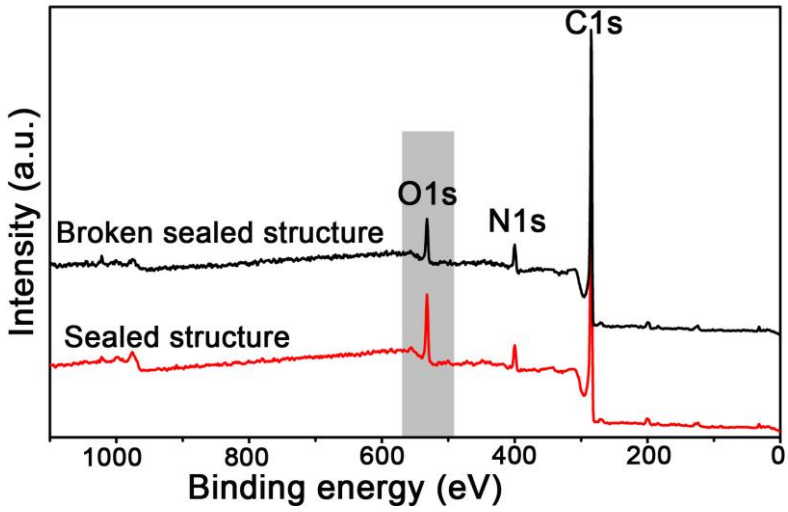

Fig. S9. XPS survey spectrum of N/O-CNCs (sealed structure and broken sealed structure)

Table S1 A comparison between the N/O-CNCs-600 and the reported carbon materials for LIBs

Material	Reversible capacity/mA h/g	Rate	Ref.
N/O-CNCs-600	**420/5, 000th cycles** **310/11, 000th cycles** **280**	**10 A/g (~26.8 C)** **30 A/g (~80.6 C)** **45 A/g (~121 C)**	**This work**
N-C-800	785/1000th cycles	5 A/g	1
CNFWs	226	20 A/g	16
PMC	205	4 A/g	17
HPNC-NS	212	37.2 A/g	18
GN	600/50th cycles	0.0744 A/g (0.2 C)	19
NCXs950-8	645/50th cycles	0.0372 A/g (0.1 C)	20
N-DHCSs	512/500th cycles	0.558 A/g (1.5 C)	21
GPF	220/5, 000 cycles	~11.2 A/g (30 C)	22
N-DCSs	870/300th cycles	0.5 A/g (~1.34 C)	23
N-doped graphene	199 (rate capcity)	25 A/g (~67.2C)	24
Hierarchically porous carbon monoliths	260/100th cycles	3.72 A/g (10 C)	25
Nitrogen-modified carbon nanostructures	853.1/800thcycles	0.5 A/g (~1.34 C)	26
Carbon nanotubes	397/100th cycles	0.1 A/g (~0.268 C)	27
N-doped G/C	359/1000thcycles	3.72 A/g (10 C)	28
Hybrid CNT and graphene	359/250th cycles	0.6 A/g (1.61 C)	29

structures			
N-3D GFs	691/500th cycles	1 A/g (~2.68C)	30
Carbon nanoribbons	750/300 cycles	0.5 A/ g (~1.34 C)	31
CNT-GN papers	330/100th cycles	0.1 A/g (~0.268 C)	32
HCNSs	772/50th cycles	0.0372 A/g (0.1 C)	33
PNCs@Gr	530/400th cycles	5A/g (~13.4 C)	34
N-MCN	604/600th cycles	2 A/g (~5.38 C)	35

Table S2 A comparison between the N/O-CNCs-600 and the reported carbon materials for SIBs

Materials	**Capacity (mAh/g), Discharge Rate (mA/g), Cyclic Stability (cycles)**	**Rate Performance**
N/O co-doped porous nanocapsules (N/O-CNCs) This Work	**340 mAh/g for 300 cylces at 0.05 A/g 230 mAh/g for 5,000 cylces at 1 A/g 150 mAh/g for 10,000 cylces at 5 A/g**	**270 mAh/g at 0.5 A/g 105 mAh/g at 10 A/g 70 mAh/g at 20 A/g**
Disodium terephthalate **(ref. S7)**	295 mAh/g at 100 cycles at 0.03 A/g	100 mAh/g at 3 A/g
Nanocellular Carbon Foams **(ref. S8)**	~140 mAh/g at 1600 cycles at 0.1 A/g	~100 mAh/g at 1 A/g ~50 mAh/g at 5 A/g
N-Doped Amorphous Carbon Nanofibers **(ref. S9)**	105 mAh/g at 500 cycles at 1 A/g	120.6 mAh/g at 1 A/g
Lithium-Pretreated Hard Carbon **(ref. S10)**	~220 mAh/g at 100 cycles at 0.05 A/g ~150 mAh/g at 1000 cycles at 1A/g	-
Osiers-sprout-likeheteroatom-doped carbon nanofibers **(ref. S11)**	160 mAh/g at 900 cycles at 0.8 A/g	~140 mAh/g at 2 A/g
Hard Carbon **(ref. S12)**	360 mAh/g at 100 cycles at 0.02 A/g	-
Hard Carbon Microtubes **(ref. S13)**	305 mAh/g at 100 cycles at 0.03 A/g	275 mAh/g at 0.15 A/g 180 mAh/g at 0.3 A/g
Hard Carbon Microspheres **(ref. S14)**	-	97 mAh/g at 0.56 A/g

		73 mAh/g at 1.4 A/g
Natural Graphite **(ref. S15)**	127 mAh/g at 300 cycles at 0.1 A/g ~103 mAh/g at 2500 cycles at 0.5 A/g	75 mAh/g at 10 A/g
		348.7 mAh/g at 0.5 A /g
Reduced Graphene foam **(ref. S16)**	329.6 mAh/g at 150cycles at 0.5 A/g	178.3 mAh/g at 1 A/g
		10.5 mAh/g at 5 A/g
Sodium 4,4′-stilbene-dicarboxylate **(ref. S17)**	112 mAh/g at 400 cycles at 1 A/g	90 mAh/g at 5 A/g 72 mAh/g at 10 A/g
Carbon nanofibers **(ref. S18)**	245 mAh/g at 280 cycles at 0.05 A/g	-
Expanded graphite **(ref.S19)**	184 mAh/g for 2000 cycles at 0.1 /g	91 mAh/g at 0.2 A/g
Carbon nanobubbles **(ref. S20)**	120 mAh/g at 30 cycles at 0.1 A/g 60 mAh/g1 at 30cycles at 0.2 A/g	25 mAh/g at 0.5 A/g
		238 mAh/g at 0.5 A /g
Carbon from Banana Peel **(ref. S21)**	298 mAh/g at 300 cycles at 0.1 A/g	155 mAh/g at 1 A/g 70 mAh/g at 5 A/g
		203 mAh/g at 0.5 A /g
Carbon Nanosheet Frameworks **(ref. S22)**	203 mAh/g at 200 cycles at 0.1 A/g	150 mAh/g at 1 A/g 66 mAh/g at 5 A/g
Hollow Carbon Nanowires **(ref. S23)**	200 mAh/g for 200 cycles at 0.125 A/g 206.3 mAh/g for 400 cycles at 0.05 A/g	149 mAh/g at 0.5 A /g
Hollow carbon nanospheres **(Ref. S24)**	160 mAh/g for 100cylces at 0.1A/g	142 mAh/g at 0.5 A/g 50 mAh/g at 10 A/g

Table S3 Composition of the N/O-CNCs-600

	Elemental analysis (wt%)			XPS % of total N1s		
	C	N	H	N-6	N-5	N-Q
N-HRCNCs-600	67.4	6.6	1.8	42.6	51.8	5.5

Table S4 Pore (> 2 nm) characteristic of the N/O-CNCs-600

	S_{BET} (m^2/g)	Total pore valume (cm^3/g)	Adsorption average pore width (4V/A by BET) (nm)
N-HRCNCs -600	471.6	0.5	4.9

Table S5 Composition of the N/O-CNCs (N/O-CNCs-500 and N/O-CNCs-700)

	Elemental analysis (wt%)			XPS % of total N1s		
	C	N	H	N-6	N-5	N-Q
N/O-CNCs-500	62.3	6.8	2.6	34.8	59.8	5.3
N/O-CNCs-700	71.1	5.4	2.0	48.4	54.7	6.8

Table S6 Pore (> 2 nm) characteristic of the N/O-CNCs-500 and N/O-CNCs-700

	S_{BET} (m^2/g)	Total pore valume (cm^3/g)	Adsorption average pore width (4V/A by BET) (nm)
N/O-CNCs -500	464.4	0.5	4.8
N/O-CNCs -700	525.6	0.5	4.0

References

S1 Y. Song, X. Shao, Z. Guo, J. Zhang, *J. Phys. D: Appl. Phys.* **2013**, *46*, 105307.

S2 M. Park, X. Zhang, M. Chung, G. B. Less, A. M. Sastry, *J. Power Sources* **2010**, *195*, 7904.

S3 Y. Qi, H. Guo, L. G. Jr. Hector, A. Timmons, *J. Electrochem. Soc.* **2010**, *157*, A558.

S4 X. Zhang, W. Shyy, A. M. Sastry, *J. Electrochem. Soc.* **2007**, *154*, A910.

S5 Y. T. Cheng, M. W. *J. Power Sources* **2009**, *190*, 453.

S6 R. Deshpande, Y. T. Cheng, M. W. Verbrugge, *J. Power Sources* **2010**, *195***,** 5081.

S7 Y. Park, D. S. Shin, S. H. Woo, N. S. Choi, K. H. Shin, S. M. Oh, K. T. Lee, S. Y. Hong, *Adv.d Mater.* **2012**, *24*, 3562.

S8 Y. Shao, J. Xiao, W. Wang, M. Engelhard, X. Chen, Z. Nie, M. Gu, L. V. Saraf, G. Exarhos, J. G. Zhang, J. Liu, *Nano Lett.* **2013**, *13*, 3909.

S9 R. Hao, Y. Yang, H. Wang, B. Jia, G. Ma, D. Yu, L. Guo, S. Yang, *Nano Energy* **2018**, *45*, 220.

S10 B. Xiao, F. A. Soto, M. Gu, K. S. Han, J. Song, H. Wang, M. H. Engelhard, V. Murugesan, K. T. Mueller, D. Reed, V. L. Sprenkle, P. B. Balbuena, X. Li, *Adv. Energy Mater.* **2018**, *8*, 1801441.

S11 H. Zhang, G. Zhang, Z. Li, K. Qu, H. Shi, Q. Zhang, H. Duan, J. Jiang, *Nano Res.* **2018**, *11*, 3791.

S12 L. Xiao, H. Lu, Y. Fang, M. L. Sushko, Y. Cao, X. Ai, H. Yang, J. Liu, *Adv. Energy Mater.* **2018**, *8*.

S13 Y. Li, Y.-S. Hu, M.-M. Titirici, L. Chen, X. Huang, *Adv. Energy Mater.* **2016**, *6*.

S14 Z. Jian, Z. Xing, C. Bommier, Z. Li, X. Ji, *Adv. Energy Mater.* **2016**, *6*.

S15 H. Kim, J. Hong, Y. U. Park, J. Kim, I. Hwang, K. Kang, *Adv. Funct. Mater.* **2015**, *25*, 534.

S16 J. T. Xu, M. Wang, N. P. Wickramaratne, M. Jaroniec, S. X. Dou, L. M. Dai, *Adv. Mater.* **2015**, *27*, 2042.

S17 C. L. Wang, Y. Xu, Y. G. Fang, M. Zhou, L. Y. Liang, S. Singh, H. P. Zhao, A.

Schober and Y. Lei, *J. Am. Chem. Soc*. **2015**, *137*, 3124.

S18 Y. Liu, F. F. Fan, J. W. Wang, Y. Liu, H. L. Chen, K. L. Jungjohann, Y. H. Xu, Y. J. Zhu, D. Bigio, T. Zhu, C. S. Wang, *Nano Lett.* **2014**, *14*, 3445.

S19 Y. Wen, K. He, Y. J. Zhu, F. D. Han, Y. H. Xu, I. Matsuda, Y. Ishii, J. Cumings, C. S. Wang, *Nat. Commun.* **2014**, *5*, 4033.

S20 H. W. Song, N. Li, H. Cui, C. X. Wang, *Nano Energy* **2014**, *4*, 81.

S21 E. M. Lotfabad, J. Ding, K. Cui, A.Kohandehghan, W. P. Kalisvaart,M. Hazelton, D.Mitlin, *ACS Nano* **2014**,*7*, 7115.

S22 J. Ding,H. L. Wang, Z. Li, A. Kohandehghan,K. Cui, Z. W. Xu, B. Zahiri, X. H. Tan, E. M. Lotfabad, B. C. Olsen,D. Mitlin, *ACS Nano* **2013**, *12*, 11004.

S23 Y. L. Cao, L. F. Xiao, M. L. Sushko, W. Wang, B. Schwenzer, J. Xiao, Z. M. Nie, L. V. Saraf, Z. G. Yang, J. Liu, *Nano Lett.* **2012**, *12*, 3783.

S24 K. Tang, L. J. Fu, R. J. White, L. H. Yu, M. M.Titirici, M. Antonietti, J. Maier, *Adv. Energy Mater.* **2012**, *2*, 873